Heterogeneous $TiO_2/V_2O_5/$ carbon nanotube electrodes for lithium ion batteries

Heterogeneous TiO_2/V_2O_5/Carbon Nanotube Electrodes for Lithium-Ion Batteries

*Mert Kurttepeli[1, ‡], Shaoren Deng[2, ‡], Felix Mattelaer[2, ‡], Daire J. Cott[3], Philippe Vereecken[3], Jolien Dendooven[2], Christophe Detavernier[2] and Sara Bals[1, *]*

[1] Department of Physics, Electron Microscopy for Materials Science (EMAT), University of Antwerp, Groenenborgerlaan 171, B-2020 Antwerp, Belgium

[2] Department of Solid State Sciences, Ghent University, Krijgslaan 281 S1, B-9000 Gent, Belgium

[3] IMEC, Kapeldreef 75, B-3001 Leuven, Belgium

KEYWORDS lithium-ion batteries, titanium dioxide, vanadium pentoxide, atomic layer deposition, transmission electron microscopy, EDX-STEM tomography.

ABSTRACT

Vanadium pentoxide (V_2O_5) is proposed and investigated as a cathode material for lithium-ion (Li-ion) batteries. However, the dissolution of V_2O_5 during the charge/discharge remains as an issue at the V_2O_5-electrolyte interface. In this work, we present a heterogeneous nanostructure with carbon nanotubes supported V_2O_5/titanium dioxide (TiO_2) multilayers as electrodes for thin-film Li-ion batteries. Atomic layer deposition of V_2O_5 on carbon nanotubes provides enhanced Li

storage capacity and high rate performance. An additional TiO_2 layer leads to increased morphological stability and in return higher electrochemical cycling performance of V_2O_5/carbon nanotubes. The physical and chemical properties of TiO_2/V_2O_5/carbon nanotubes are characterized by cyclic voltammetry and charge/discharge measurements as well as electron microscopy. The detailed mechanism of the protective TiO_2 layer to improve the electrochemical cycling stability of the V_2O_5 is unveiled.

1. Introduction

Lithium-ion batteries (LIBs) are excellent power sources for a variety of applications, such as wearables, medical implants, wireless sensors and smart textiles due to their small form factor and high energy density.[1] By using thin films as electrodes, the ionic and electronic pathways in the battery are much shorter and more efficient, which enables the use of high power applications that require fast charging and discharging. The disadvantage of using thin films is their low storage capacity due to their limited thickness. However, this can be overcome by the application of thin-film electrodes on a complex 3D substrate, with an enhancement of the capacity enabled by the available surface enhancement.[2-5] In this respect, carbon nanotubes (CNTs) are a well-known template for high-energy and high-power applications, because of their high surface area and their ability to function as an excellent current collector. However, a fully conformal coating technique is required to enable the use of CNTs as a template for 3D thin film LIBs. As a result of the self-limiting nature of the reactions between the gas-phase precursor and the substrate, atomic layer deposition (ALD) is the ideal technique to reach this goal.[6-10] Indeed, ALD metal oxide layers, such as vanadium pentoxide (V_2O_5) or titanium dioxide (TiO_2), deposited onto CNTs templates have already been proven to be useful as electrode materials.[11-17]

Vanadium oxides and more specifically V_2O_5 have been widely investigated as LIB cathode materials. V_2O_5 layers are of great interest due to their high specific capacity, natural abundance, and lower toxicity in comparison to currently used cathode materials.[18-23] Generally, V_2O_5 is not considered ideal as a cathode for a classical lithium ion battery due to its moderate electronic conductivity (10^{-3}–10^{-2}S cm) and low lithium diffusion coefficients (10^{-13}–10^{-12} cm² s^{-1}).[24-27] For short diffusion paths, such as thin-film cathodes, on top of good conductivity 3D templates, such as CNTs, these limitations can be overcome.[28, 29] In fact, summarized in a recent review by Huang

et al, nanostructuring is one of the three main strategies to enable the use of vanadium pentoxides, alongside carbon hybridization and cation doping.[30] Up to 3 lithium ions can be stored in V_2O_5, yielding a theoretical capacity of 442 mAh/g, well above the capacity of $LiCoO_2$, which is traditionally used as cathode in commercial LIBs. However, only the insertion of one lithium ion is found to be reversible, due to breaking of chemical bonds upon further lithiation, initiating vanadium dissolution and breakdown of the crystal structure.[31, 32] Metal ion dissolution is not only an issue for V_2O_5, but is a significant factor in capacity fade in many cathode materials, for example in $LiMn_2O_4$.[33]

Protective coatings have been found to alleviate this issue largely. So far, Al_2O_3 buffer layers have been mostly used, since these layers have a protective function against solid-electrolyte interphase (SEI) formation at the anode side[34-36] and metal dissolution at the cathode side.[37, 38] However, Al_2O_3 is essentially ionically blocking, so this coating is a kinetic bottleneck that can only offer the desired protective function if the layer is made ultra-thin (<1 nm).[38, 39] Thus, the protective function of Al_2O_3 ensuring no loss in energy density causes a loss in power density. Other coating materials that are not ionically blocking, such as TiO_2, can also be deposited using ALD and they show similar protective functions, while the compromise in power density can be avoided.[17, 34, 40, 41] For example, it was shown that applying a 2-3 nm layer of ALD TiO_2 on graphite improves the diffusion coefficient for lithium ions.[34] It was furthermore shown that a layer of up to 30 nm TiO_2 enhances the rate performance and the capacity retention in graphite, indicating that the TiO_2 layer does not become a kinetic bottleneck even at higher thicknesses, while at the same time the capacity retention properties are improved.[41] Recently, Xie et al reported the first work dealing with ALD TiO_2 on amorphous V_2O_5 coated on CNTs as a protective coating to deal with the vanadium dissolution.[17] They showed improvement in electrochemical cyclability in the 1.5-

4.0V vs Li^+/Li region, however, within this potential region TiO_2 itself also inserts lithium, degrading the stability over long term cycling. [37]

Here, we investigate CNT-supported ALD crystalline V_2O_5 cathodes in the medium charge-discharge regime (down to 2.0V vs Li^+/Li, lithiating V_2O_5 to $Li_2V_2O_5$). This paper reports the balance between performance and capacity as a function of the thickness of ALD deposited TiO_2 layers on V_2O_5/CNTs cathodes. By using advanced electron microscopy techniques, such as energy dispersive X-ray spectroscopy-scanning transmission electron microscopy (EDX-STEM) tomography, the complex 3D structure and composition of the TiO_2 and V_2O_5 layers is characterized. Our results show that a remarkable rate capability and stable electrochemical cyclic performance is achieved from these TiO_2/V_2O_5/CNTs layered nanomaterials. Our measurements furthermore reveal that the thickness of the TiO_2 layer has a significant effect on the stability of the V_2O_5/CNTs cathodes by affecting the phase transition of V_2O_5, as well as resolving the vanadium dissolution issues.

2. Experimental Procedures

2.1 Carbon nanotubes growth on Silicon substrate

Multi-walled CNTs (MWCNTs) were grown from a 1nm (nominal) Co catalyst layer deposited on a Si wafer with a diameter of 200 mm. To avoid diffusion of the Co into the Si, a 70 nm TiN was first sputter deposited onto the Si surface (Endura PVD tool, Applied Materials, USA). MWCNTs were grown in a microwave (2.45 GHz) plasma enhanced chemical vapor deposition chamber (PECVD, TEL, Japan). In a typical experiment the Co catalyst layer was exposed to a NH_3 plasma for 5 minutes to transform the film into active metal nanoparticles for CNT growth. Then a C_2H_4/H_2 mixture was flowed into the chamber at a temperature >550° C for 30 minutes.[42]

2.2 ALD-based coatings of TiO_2-VO_x-TiO_2 layers

MWCNTs were loaded into a homemade ALD system with a base pressure of $2*10^{-7}$ mbar. Metalorganic precursors and water (for VO_x)/ozone (for TiO_2) were alternatively pulsed into the chamber while the MWCNTs sample was heated up to 150°C in case of VO_x and 100°C in case of TiO_2. Tetrakis-(ethylmethylamino) vanadium (TEMAV) (Air Liquide) and Tetrakis-(dimethylamido) titanium (TDMAT) (99.9%, Sigma Aldrich) were used as metal precursors for VO_x and TiO_2, respectively.[43, 44] To achieve a conformal coating on the MWCNTs forest, 20-30 seconds precursor pulses at a pressure of 0.4~0.5 mbar were applied. The pumping time was chosen as twice the pulse time to ensure sufficient evacuation of the residual precursor vapor and reaction products, thus avoiding chemical vapor deposition inside the forest of CNTs. 85 ALD-cycles have been applied on the CNTs template for VO_x coating. In a home-modified *in situ* XRD system (Bruker D-8) with heating stage, prior to ALD of TiO_2, VO_x/CNTs arrays were annealed from 20°C to 325°C at a rate of 5°C per minute in air and kept at 325°C for 1 hours for the phase transformation of VO_x coating into V_2O_5. Subsequently, 5 and 25 ALD-cycles have been applied on the V_2O_5/CNTs for TiO_2 coating in order to obtain different thicknesses. The schematic representation of the synthesis route applied to the materials investigated here can be found in the supplementary information (SI) Figure S1.

2.3 SEM and TEM characterizations

Cross-sections of the uncoated V_2O_5/CNTs and TiO_2/V_2O_5/CNTs were characterized using a scanning electron microscope (SEM-FEI Quanta) in order to resolve the morphology of the nanotube forests. Transmission electron microscopy (TEM) specimens were prepared from the samples and studied with a variety of techniques in order to obtain more detailed information. Samples were prepared by scraping off the Si wafer surface and suspending the resulting powder

in ethanol. A drop of this suspension was deposited on a carbon coated TEM grid. High-resolution TEM (HRTEM) was performed using a FEI Osiris operated at 200 kV. High-angle annular dark field scanning TEM (HAADF-STEM) images and energy-dispersive X-ray (EDX) elemental maps were collected using an aberration corrected cubed FEI Titan operated at 200 kV, equipped with a Super-X detector for EDX analysis.

2.4 EDX-STEM tomography experiments

An aberration corrected cubed FEI Titan microscope equipped with a Super-X detector was used to acquire EDX elemental maps and to perform simultaneous HAADF-STEM at an acceleration voltage of 120 kV. Tilt series were acquired using an advanced tomography holder from Fischione Instruments (Model 2020). The hybrid nanomaterial system in our study consists of constitutional elements such as C, O, Ti and V with atomic numbers (Z) of 6, 8, 22 and 23, respectively. Elemental maps were obtained by scanning of individual frames of same location and summing multiple frames with a constant dwell time for different tilt angles. Data acquisition consisted of a EDX-STEM tomography procedure where each 256×256 pixels elemental maps were acquired for constant collection times using Bruker Esprit™ software together with simultaneous HAADF-STEM images. The elemental maps were acquired at a beam current of 0.2 nA. The total acquisition time was ~4 h which is the total duration for simultaneous HAADF- and EDX-STEM tilt series acquisition including the tracking/focusing. Each tomography tilt series consisted of 31 HAADF images and EDX maps for each element acquired over a tilt range of ±75° using a tilt increment of 5°. Alignment of the data was carried out by cross correlation as implemented in the FEI Inspect3D software package. The reconstruction was performed using the "Simultaneous Iterative Reconstruction Technique" (SIRT) with 25 iterations implemented in FEI Inspect3D. Amira (Visage Imaging GmbH) was used for visualization of the reconstructed volume.

2.5 Electrochemical testing of TiO_2/V_2O_5/CNTs electrodes

Electrochemical measurements were performed using a custom-built three-electrode Teflon cell. The Teflon cell was clamped onto 2cm×2cm samples using a Viton O-ring. The geometrical surface area of the exposed electrode was 0.9503 cm^2. A lithium metal sheet and a wire were used as a counter and reference electrode, respectively. The Li reference electrode was placed in a capillary with the tip placed less than 1mm from the electrode surface. Contact was made to the bare TiN under layer with a crocodile clip at the edge of the sample (outside of the glass cell). The electrolyte used was 1.0M $LiClO_4$ in propylene carbonate (PC) (99%, IoLiTec) All of the operations on the cell assembly were carried out in a glove box filled with argon gas in which both the water and oxygen concentrations were less than 1 ppm. A potentiostat/galvanostat Autolab PGSTAT302 (Metrohm Autolab) was used to perform all of the electrochemical experiments, which were controlled through Nova 1.8 software. All of the voltages are given versus the Li^+/Li.

Cyclic voltammograms (CV) were recorded starting from the open-circuit potential between 4.00V and 2.00V vs Li^+/Li at a scan rates of $10mVs^{-1}$. Subsequently, galvanostatic cycling was performed between 4.00V–2.00V at various current densities (C-rates) to evaluate the rate and electrochemical cycle performance. For the charging rate, 1C was determined based on the charge calculated from the discharge capacity with a $0.5mVs^{-1}$ CV. To account for variations in the CNT densities on the substrate, the measured capacities were scaled to the amount of vanadium deposited, as determined by XRF. Unscaled capacities are shown in the supporting information.

3. Results and Discussion

3.1 Structure and morphology of the V_2O_5-coated CNTs

To crystallize the VO_x, ALD coated MWCNTs samples were loaded into a home modified *in situ* XRD system and annealed in air at 325ºC for 1 hour. The diffraction peaks were monitored

during the annealing, as shown in Figure 1-(a). The isothermal process at 325°C was specifically chosen to crystalize the VO_x to V_2O_5 but not to oxidize the MWCNTs and the TiN layer underneath, since in a previous study, it was shown that the oxidation temperature of VO_x coated MWCNTs is about ~400°C.[37] It can be seen in Figure 1-(a) that the V_2O_5 peaks appear when the temperature reaches 325°C whereas the peaks from the TiN layer do not disappear during the annealing. The diffraction peaks in the *ex situ* XRD pattern as shown in Figure 1-(b) indicate that VO_x was crystallized into V_2O_5 with *Pmmm* space group and since no detectable TiO_2 peaks were observed, a good preservation of TiN is expected.

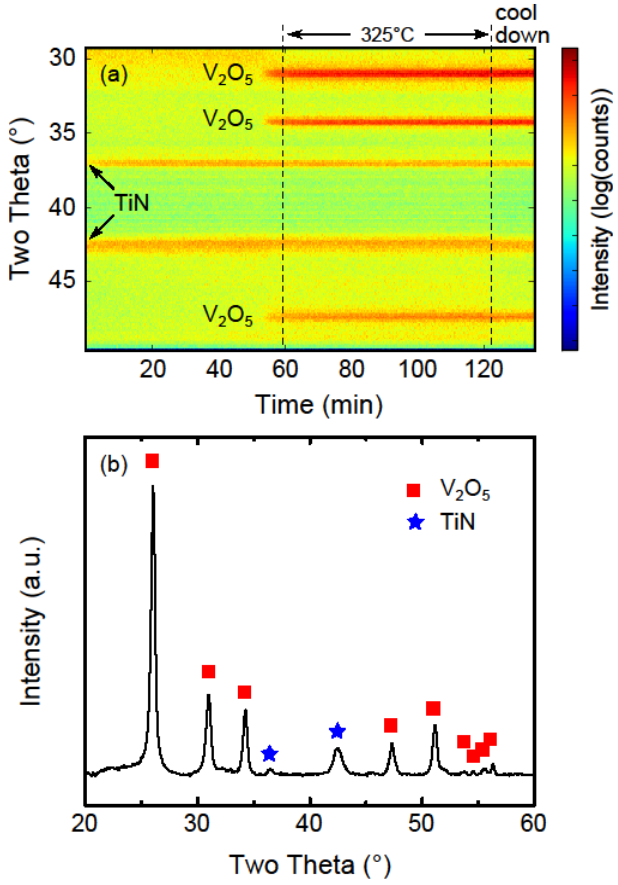

Figure 1. *In situ* (a) and *ex situ* (b) XRD results of VO_x coated CNTs annealed in air at 325°C for 1 hour.

A SEM image of the 85 cycles ALD V_2O_5 coated CNTs arrays on the TiN/SiO_2/Si substrate after annealing in air environment is presented in Figure 2-(a). From the cross-sectional SEM image, it can be seen that the material constitutes a porous structure composed of thin, tubular and branched features occasionally linked to each other. A more detailed investigation of the sample was performed by TEM. From the HRTEM image (see Figure 2-(b)), it is clear that the graphitic layers of CNTs are surrounded by a thin, crystalline coating. The interplanar spacing between two layers in CNTs corresponds approximately to 0.34 nm, which is the typical distance between two graphene layers in graphite. Such appearance of graphene layers suggests the preservation of MWCNTs subsequent to the annealing process. In addition, HRTEM indicates that the annealing of the as-deposited VO_x on CNTs in air environment results in the transformation from amorphous VO_x into V_2O_5 crystalline form, while the MWCNTs are preserved. On the other hand, HRTEM showed that the ALD VO_x coating was not completely uniform, and that MWCNTs without coated regions are occasionally observed, as shown in Figure 2-(c).

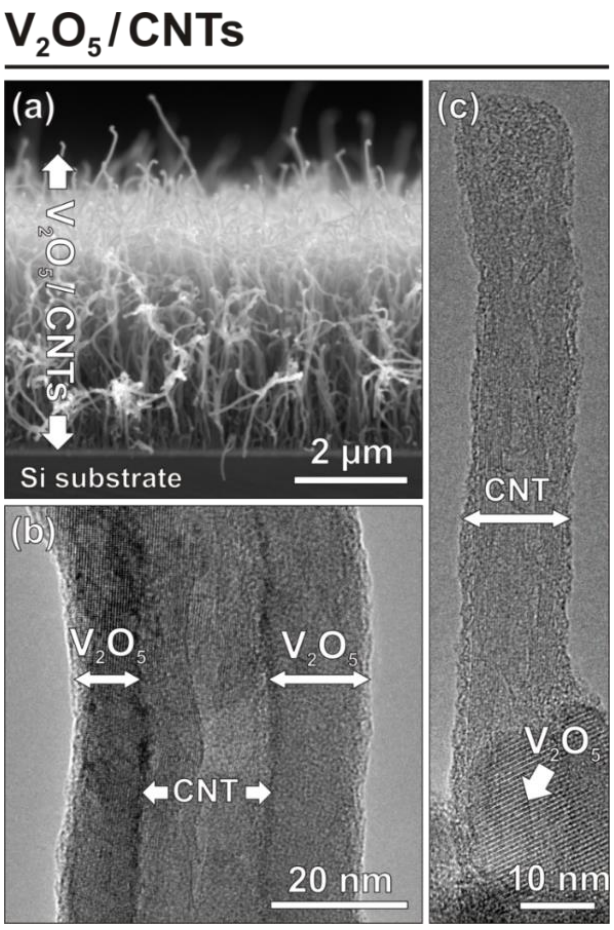

Figure 2. (a) SEM image of uncoated V_2O_5/CNTs from cross-sectional view is given. HRTEM images given at (b) and (c) reveal the structure of V_2O_5/CNTs before the LIB tests.

3.2 ALD coating of TiO_2 on V_2O_5/CNTs

As stated earlier, by changing the number of ALD cycles between 5 and 25, TiO_2 layers with varying thicknesses were deposited onto V_2O_5/CNTs. For instance, after 25 ALD cycles of TiO_2 deposition, a structure as illustrated by the SEM image in Figure 3-(a) is obtained. The SEM image shows that the overall forest-type morphology was preserved after ALD of TiO_2. A HRTEM image (see Figure 3-(b)) from the same sample reveals that an amorphous TiO_2 layer is surrounding the crystalline V_2O_5/CNTs. In a similar way, 5 ALD cycles TiO_2 coating appeared to be in its amorphous form, which was revealed by TEM. In terms of crystallinity, ALD of TiO_2 hereby

shows similar result with respect to one of our previous studies, in which the as-deposited ALD processed TiO_2 film on a carbon nanosheet template showed likewise no crystallinity upon its deposition.[45] The HAADF-STEM image in Figure 3-(c) shows the presence of tubular-shaped nanostructures. To illustrate the distribution of the elements in the sample, elemental mapping by EDX was performed for the region indicated in Figure 3-(c). Figure 3-(d-h) shows the local elemental distributions of C, O, V and Ti at the sample. From the results, the TiO_2 coating appears to be uniformly surrounding the V_2O_5 coated CNTs. However, it should be noted that these images and elemental maps only correspond to 2D projections of a 3D object. Therefore, in order to retrieve the correct 3D (chemical) information, EDX-STEM tomography was used.

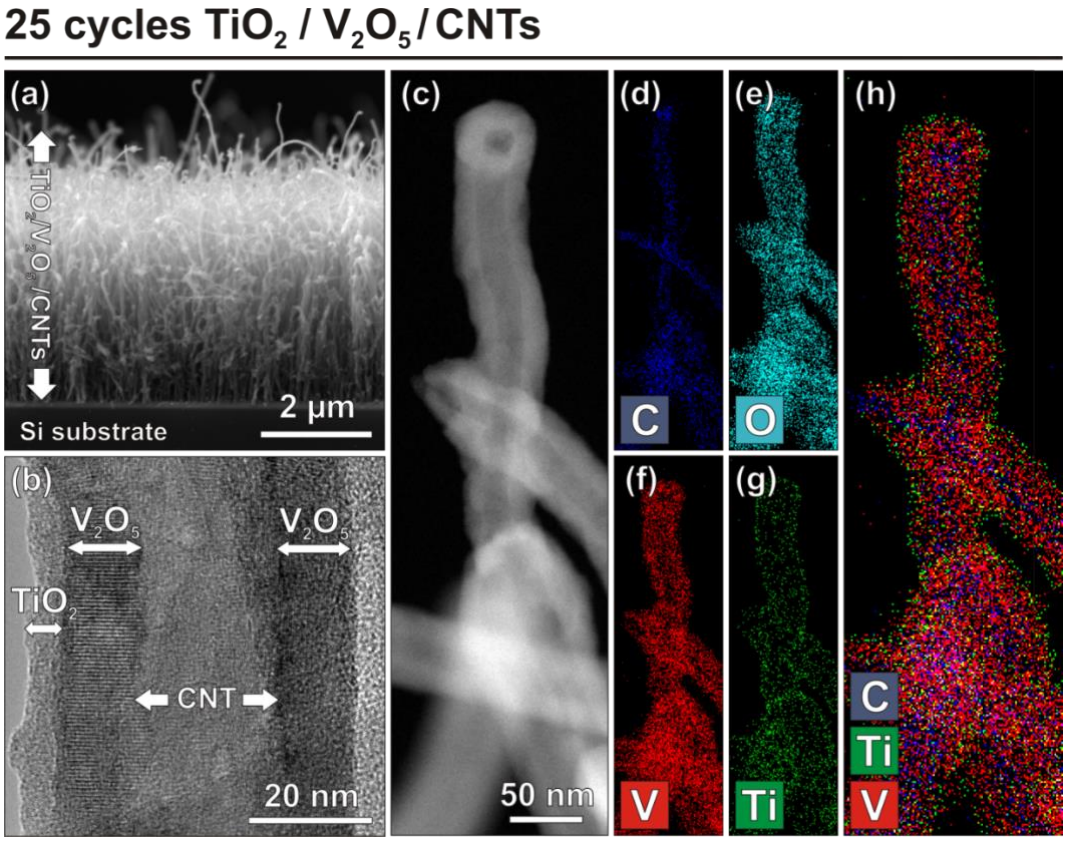

Figure 3. (a) SEM image of 25 ALD cycles TiO_2 coated V_2O_5/CNTs from cross-sectional view is given. HRTEM image of 25 ALD cycles TiO_2 coated V_2O_5/CNTs given at (b) reveals the structure

of both TiO_2 and V_2O_5 coatings before the LIB tests. (c) HAADF-STEM image shows individual TiO_2/V_2O_5/CNTs. (d) Carbon, (e) oxygen, (f) vanadium and (g) titanium compositions of the nanotubes can be seen on (h) EDX mixed color elemental map.

During such an experiment, 2D EDX elemental maps are collected simultaneously with HAADF-STEM images. The results of the 3D HAADF-STEM and 3D EDX-STEM reconstructions from 25 ALD cycles TiO_2 coated V_2O_5/CNTs sample prior to electrochemical cycling tests are presented in Figure 4. The individual 3D elemental distributions of Ti (green), V (red) and C (blue) as well as the superposition of the Ti, V and C signals are also shown (See Figure 4-(c–f)). The HAADF-STEM reconstruction illustrates the morphology of the tubes, but due to the small HAADF-STEM contrast between the different elements, no chemical information can be extracted from individual C, Ti and V containing layers (see Figure 4-(a-b)). On the other hand, the 3D EDX-STEM results demonstrate fine coatings of Ti and V surrounding the C containing interior (see Figure 4-(c-f)). The layers are found to be comparably homogenous although sections without coatings are also observed (see Figure 4-(d) and (e)). Such inhomogeneity at the nanoscale can be expected, since ALD is known to cause the appearance of pinholes and uncoated sections for both TiO_2, and VO_x depositions due to overlap of CNTs in MWCNTs forests.[43, 44] However, such defects can be beneficial when using these materials as cathodes, since these areas may facilitate Li^+ insertion/extraction.

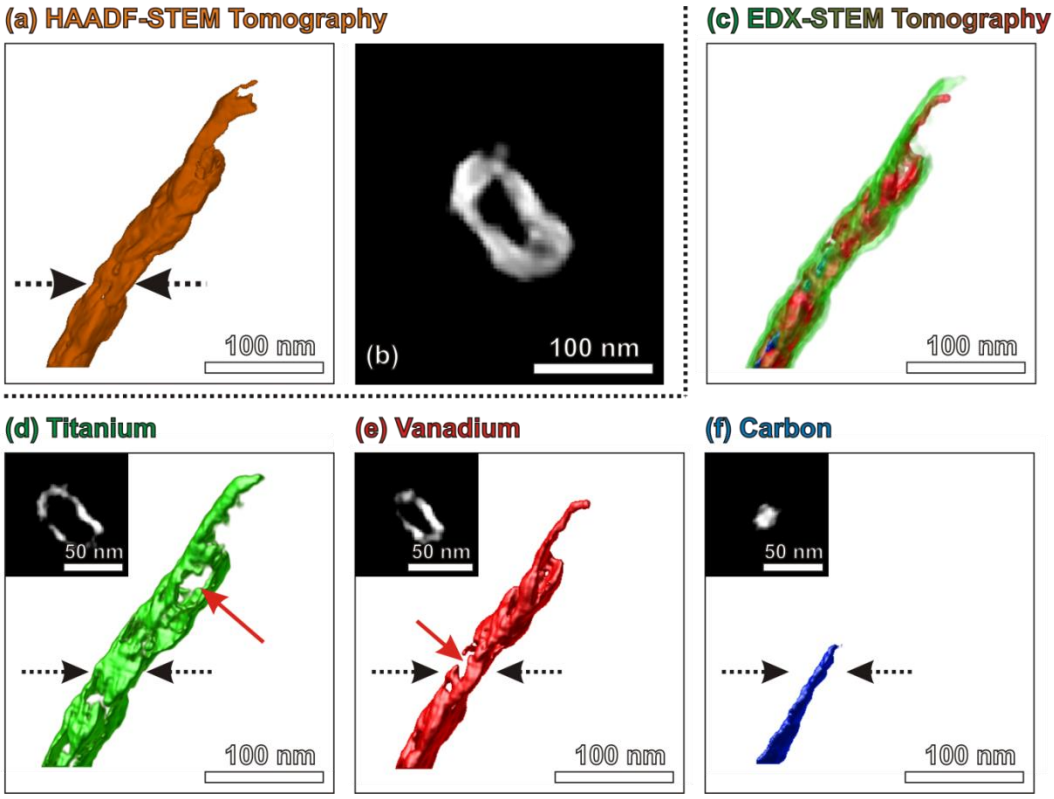

Figure 4. 3D visualizations of HAADF-STEM and EDX-STEM reconstructions from 25 ALD cycles TiO_2 coated V_2O_5/CNTs sample. (a) 3D visualization obtained by HAADF-STEM tomography and (b) an orthoslice through the 3D reconstruction. (c) Superimposition of 3D elemental distributions of Ti, V and C and individual 3D elemental distribution of (d) titanium, (e) vanadium and (f) carbon. The orthoslices of EDX-STEM reconstructions for each element are given at insets from positions indicated at the 3D visualizations by black arrows. Red arrows indicate the uncoated regions.

3.3 Electrochemical and rate performance improvement of TiO_2/V_2O_5/CNTs electrodes

The electrochemical performance of CNT-supported V_2O_5 as lithium-ion battery cathode was examined, and compared to that of the TiO_2-coated cathodes. Cyclic voltammetry was employed to evaluate the potential window for insertion and extraction of lithium in uncoated V_2O_5/CNTs as well as 5 and 25 ALD cycles TiO_2 on V_2O_5/CNTs. Figure 5 shows the CV at a scan rate of

10mVs^{-1} in the voltage window of 2.00-4.00V vs Li^{+}/Li. This potential range was carefully chosen to allow the (de)intercalation of two lithium ions per V_2O_5 unit cell,[31, 32] while remaining well above the intercalation window for TiO_2 as for not involving it to participate in the lithiation/delithiation electrochemical cycles.[46] The intercalation of two lithium ions per V_2O_5 unit cell is reported to be much less reversible than intercalation of just one, but yields a higher theoretical capacity.[31] From the CV scans of the uncoated V_2O_5/CNTs, it is observed that three reduction-oxidation peak couples are present: two centered above 3.0V vs Li^{+}/Li corresponding to the two-stage (de)intercalation of one lithium into V_2O_5, [30, 32, 47, 48] and another centered around 2.4V vs Li$^{+/}$Li corresponding to (de)intercalation of a second lithium into LiV_2O_5. The same holds for the 5 and 25 ALD cycles TiO_2 on V_2O_5/CNT samples: only the peaks corresponding to (de)intercalation into V_2O_5 are present, indicating that the TiO_2 ALD film does not contribute in the (de)intercalation reactions. For the 5 ALD cycles TiO_2 on V_2O_5/CNT sample, we observe that the peaks are slightly suppressed, and more so for the 25 ALD cycles TiO_2 on V_2O_5/CNT sample. Furthermore, the overpotential is higher for both samples, indicating the TiO_2 films may cause a kinetic bottleneck during the first electrochemical cycles.

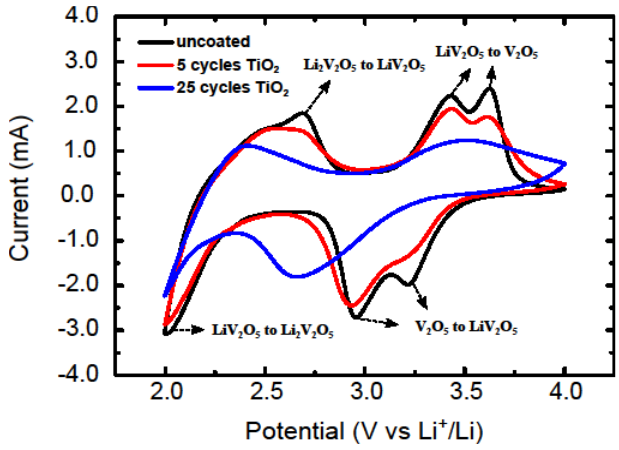

Figure 5. The third cyclic voltammograms of uncoated and 5 and 25 ALD cycles TiO_2 coated V_2O_5/CNTs at 10mVs^{-1}.

To further investigate this effect, four galvanostatic charge-discharges were performed on the same samples at different C-rates (1-100C). The current applied for each C-rate was determined from the theoretical capacity for insertion of two lithium ions into V_2O_5 (294.7mAh/g) and the amount of V_2O_5 present in each sample calculated from equivalent V_2O_5 thicknesses derived from vanadium XRF measurements. Figure 6 plots the discharge capacity for varying C-rates of uncoated, 5 and 25 ALD cycles TiO_2 coated V_2O_5/CNTs cathodes. Good kinetics were observed for all samples, with only 20-25% loss upon charging in 20C compared to 1C. Coating with 5 or 25 ALD cycles of TiO_2 improves the capacity retention noticeably up to 20C, but for high C-rates such as 100C, it is seen that the uncoated sample has a higher available discharge capacity. Therefore, it can be concluded that the TiO_2 coating slightly enhanced the kinetics of the lithiation/delithiation process at low and intermediate C-rates, and only slows down the kinetics at very high C rate. This is significantly different from reported ALD coatings on V_2O_5: Al_2O_3 in which ALD was shown to improve the electrochemical cyclability of hydrous vanadium oxide but at the same time impose a kinetic bottleneck.[42] While a TiO_2 ALD coating on V_2O_5/CNTs has already been reported to have good rate retention in the 3 lithium intercalation regime (84% at 2.3C),[17] the kinetics shown here in the 2 lithium intercalation regime are more than 5 times better (85% at 10C), enabling the use of this material as high-rate cathode.

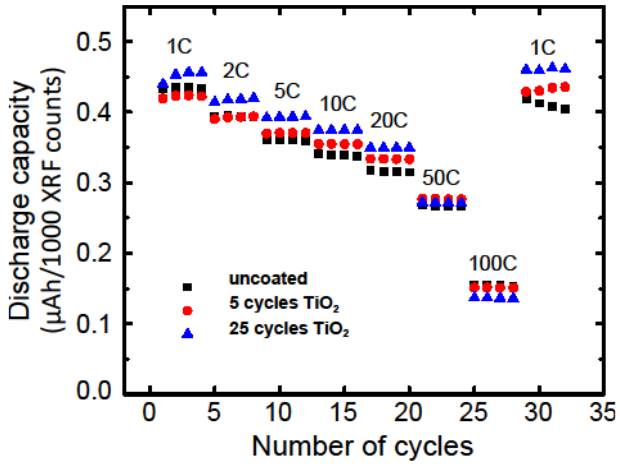

Figure 6. Discharge capacity of the kinetics at 1-100C for 30 electrochemical cycles of uncoated and 5 and 25 ALD cycles TiO_2 coated V_2O_5/CNTs. C-rates were calculated based on the measured vanadium content of the samples.

Finally, we investigated the effect of the coating on the electrochemical cyclability of the cathodes. Because of the chosen potential range, two lithium per V_2O_5 were inserted into the samples, which is beyond the reported range of full reversibility. The delithiation capacity and Coulombic efficiency evolution at 2C for the samples under investigation are shown in Figure 7. Indeed, we see a significant decrease in capacity for the uncoated V_2O_5/CNTs upon electrochemical cycling, losing almost 17% of the available delithiation capacity after 100 electrochemical cycles. There are clearly two stages in the evolution of the uncoated V_2O_5/CNTs. During the first 40 electrochemical cycles, the capacity remains almost constant, while the Coulombic efficiency is increasing from 76.7% during the first cycle to 99.5% at the 40^{th} electrochemical cycle. After the 40^{th} electrochemical cycle, the Coulombic efficiency varies between 99.5 and 100%, while the capacity fades. In fact, the fraction of the capacity that is lost during the last 60 electrochemical cycles matches very well with the fraction of Coulombic efficiency missing from 100%, indicating that a fraction of the available active material between 0.05 and 0.5% is lost every electrochemical cycle. For the sample coated with 5 ALD cycles of TiO_2, a similar two-stage behavior is seen: up to 65 electrochemical cycles the capacity remains constant, while the Coulombic efficiency slowly rises to close to 100%, and after the 65^{th} electrochemical cycle the latter remains constant while the capacity starts decreasing. It is reported for V_2O_5 that the capacity loss is related to vanadium dissolution upon overcharging. The low coulombic efficiency during the first stage indicates that more lithium is incorporated than extracted, building more and more lithium into the samples and gradually overcharging it. At a

certain point, this excess buildup of lithium is completed (40th electrochemical cycle for the uncoated V_2O_5/CNTs and 65th electrochemical cycle for the sample coated with 5 cycles of ALD TiO_2), upon which the capacity starts fading by the dissolution mechanism. Coating the V_2O_5/CNTs with 5 cycles of ALD TiO_2 seems to delay this mechanism, but does not prevent the loss of capacity completely. For the sample coated with 25 cycles of ALD TiO_2, no such two-stage mechanism is seen. Instead, the coulombic efficiency rises much faster, indicating much less excess lithium buildup or a more efficient extraction of lithium. Instead of a drop in available capacity, the capacity increases gradually during the 100 electrochemical cycles to almost 9% above the initial capacity.

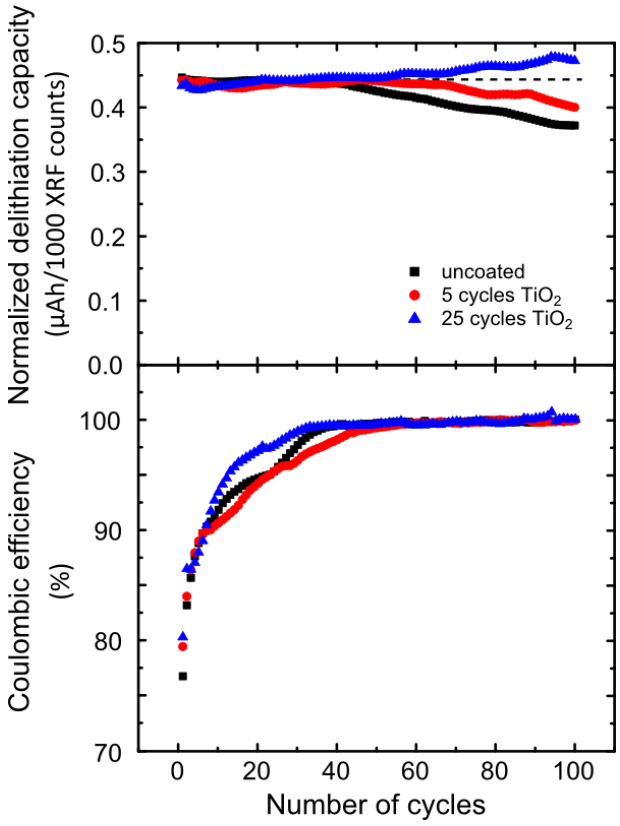

Figure 7. Cyclability testing of uncoated V_2O_5/CNTs and of 5 and 25 ALD cycles TiO_2 on V_2O_5/CNTs samples at a current corresponding to 2C between 2.0 and 4.0 V vs Li^+/Li.

3.4 Discussion of the capacity retention improvements

We observe capacity loss for the uncoated V_2O_5/CNTs and the V_2O_5/CNTs coated with 5 ALD cycles of TiO_2. The electrochemical performance (including electrochemical cyclability) of the nanostructured V_2O_5 is limited by vanadium dissolution.[50] As mentioned previously, further performance improvement of the nanostructured V_2O_5-based cathode is aimed by introducing an additional TiO_2 layer onto the V_2O_5/CNTs with various thicknesses (ALD cycles). To evaluate the effect of preventing vanadium dissolution by ALD coating, the vanadium loss induced by electrochemical cycling was examined by applying XRF characterizations on the V_2O_5/CNTs samples before and after the LIB cyclability test. The percentages of the vanadium retention were determined to be 72.9%, 83.5% and 99.6% after 100 electrochemical cycles charge/discharge for the cases of uncoated V_2O_5/CNTs, 5 ALD cycles TiO_2 coated V_2O_5/CNTs and 25 ALD cycles TiO_2 coated CNTs, respectively (see Figure 8). This demonstrates that a TiO_2 coating consisting of 25 ALD cycles is very efficient alleviating the vanadium dissolution, without imposing a kinetic bottleneck on the cathode.

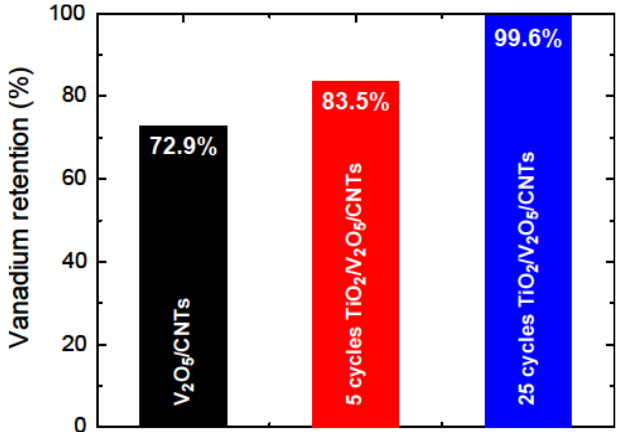

Figure 8. XRF characterizations determined vanadium retention for V_2O_5/CNTs, 5 TiO_2/V_2O_5/CNTs and 25 TiO_2/V_2O_5/CNTs samples after the cyclability test.

While the capacity retention in the coated V_2O_5/CNTs is explained by the vanadium dissolution function of the coating, the capacity of the 25 TiO_2/V_2O_5/CNTs is not only retained, but also increased almost 9% over the 100 charge-discharge cycles. This can be explained by an evolution from crystalline to amorphous structure. The charge-discharging profiles of these three cases are shown in Figure 9, and their derivatives (dQ/dV) in supplementary information (Figures S4-S6). During the first electrochemical cycles, three clear plateaus (or sharp peaks in the dQ/dV plots) can be seen for all samples, corresponding to the three-stage (de)lithiation of V_2O_5 as shown on the cyclic voltammograms. For the 25 ALD cycles-coated V_2O_5/CNTs the first lithiation plateau at 3.4V is shifted to lower potential, but still identifiable from the dQ/dV profile (S5). These sharply aligned (de)lithiation regions are present due to the crystalline nature of the V_2O_5, and correspond to the overcoming of energy barriers within the crystal lattice. After 100 charge-discharge electrochemical cycles, the uncoated and 5 ALD cycles-coated V_2O_5/CNTs samples still show the characteristic plateaus and corresponding peaks in the charge-discharge profiles and dQ/dV's, respectively. In the 25cycles ALD TiO_2 coated V_2O_5/CNTs, all signs of those are lost. This indicates no crystal structure is left after 100 (de)lithiation electrochemical cycles for the latter. For many materials, it has been shown that an amorphous material is able to store more lithium and has faster kinetics than the crystalline counterpart.[17, 51-53] The amorphisation of V_2O_5 when coated with 25 cycles of ALD TiO_2 thus explains the rise in capacity upon electrochemical cycling and gradual amorphisation. Since these films are also coated with ALD TiO_2, the vanadium dissolution is also inhibited, preventing capacity loss while at the same time improving the kinetics upon electrochemical cycling.

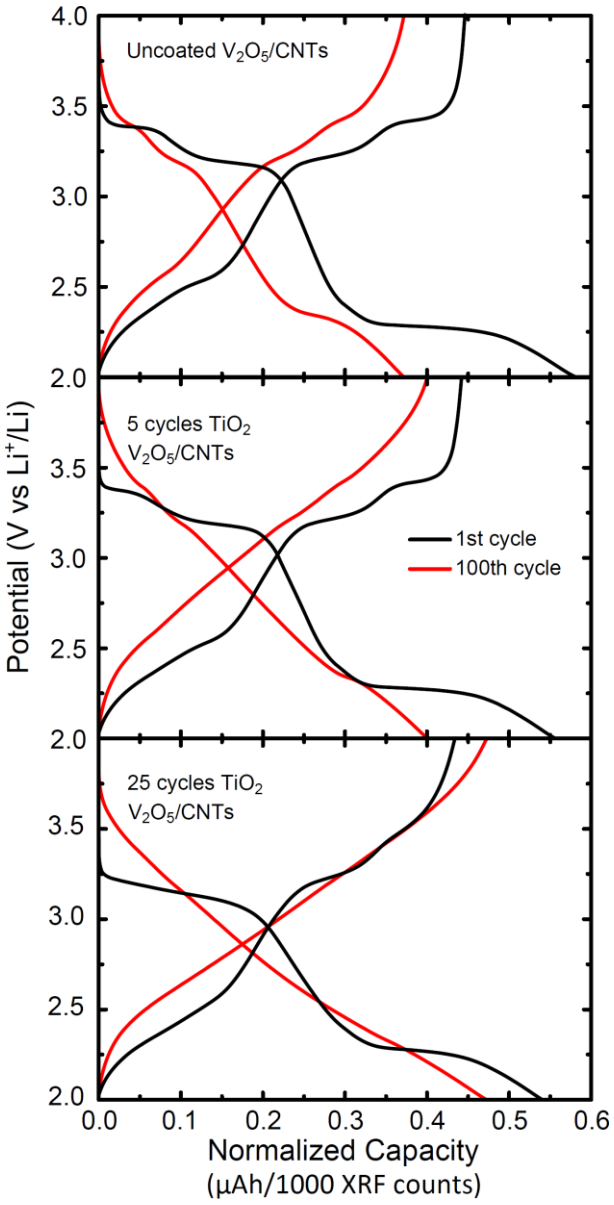

Figure 9. Charge-discharge profiles of the first and last electrochemical cycle of the cyclability experiment

To investigate this amorphisation, the post- electrochemical cycling samples were investigated by SEM, TEM and XRD in the same manner as for as-synthesized samples. SEM image of the uncoated V_2O_5/CNTs sample after the LIB tests shows that the morphology of the material was substantially preserved (see Figure 10-(a)). HRTEM indicates that the crystalline V_2O_5 coating

became amorphous (see Figure 10-(b)), contrary to what was expected from the electrochemical measurements. Investigations of the samples with 5 and 25 cycles TiO_2 on V_2O_5/CNTs show similar results. SEM image of the 25 cycles TiO_2 on V_2O_5/CNTs reveals that the overall forest-type morphology is preserved (see Figure 10-(c)) and from the HRTEM image (see Figure 10-(d)) the amorphous V_2O_5 coating can be observed, which was also the case for both uncoated V_2O_5/CNTs and 5 cycles TiO_2 on V_2O_5/CNTs samples. As seen in Figure 10-(e-h), EDX mapping on the samples with TiO_2 coated V_2O_5/CNTs indicates that the VO_x/CNTs are still perfectly protected by TiO_2 without structural collapse. EDX-STEM analysis hereby indicated that the morphology and chemistry of the TiO_2 coated V_2O_5/CNTs did not change significantly, when the individual EDX elemental maps before and after the cyclability test were compared (see Figure 3-(d-h)).

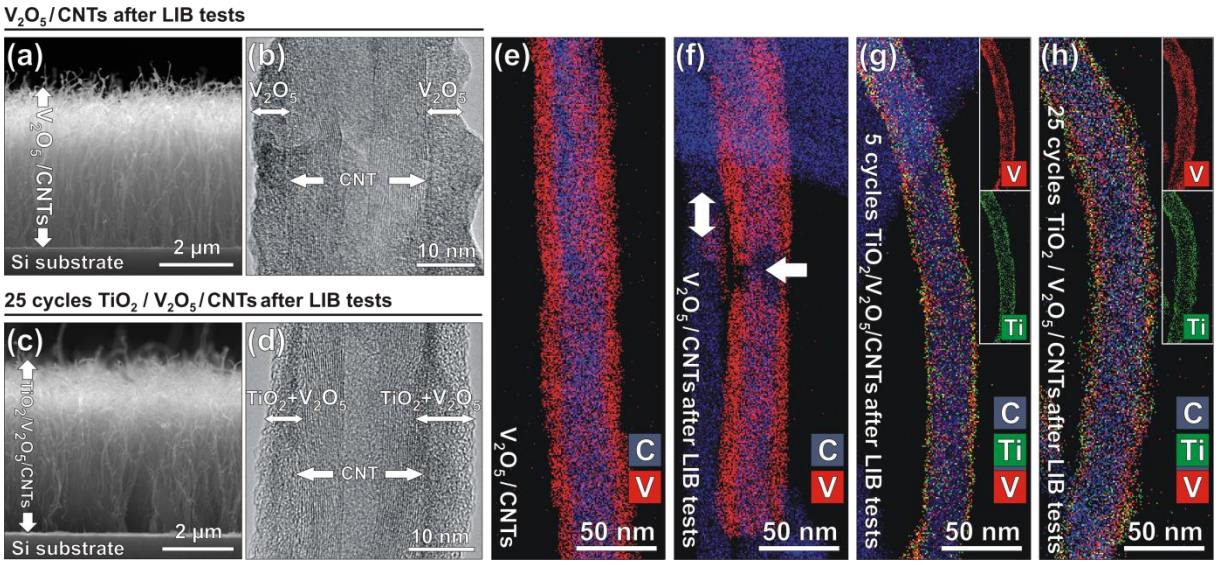

Figure 10. (a) SEM image of V_2O_5/CNTs from cross-sectional view after the cyclic voltammetry is given. HRTEM image given at (b) reveals the structure of V_2O_5/CNTs after the cyclic voltammetry tests. (c) SEM image of TiO_2/V_2O_5/CNTs from cross-sectional view after the cyclic voltammetry tests is given. HRTEM image given at (d) reveals the structure of both TiO_2 and V_2O_5

coatings after the cyclic voltammetry tests. (e-h) shows the EDX mapping of V_2O_5/CNTs sample before and V_2O_5/CNTs, 5 and 25 ALD cycles TiO_2 coated V_2O_5/CNTs samples after cyclability test.

To further investigate the degree of crystallinity post- electrochemical cycling, XRD patterns of the samples were investigated (see Figure 11). It is clear that all samples remain crystalline to some extent, although direct comparison before and after electrochemical cycling was not possible due to sample handling. However, a sample-to-sample comparison allows elaborating to the degree of crystallinity left in the samples. A peak identification was performed, and much more V_2O_5 peaks are visible post- electrochemical cycling compared to before (see Figure 1), indicating restructuring of the V_2O_5 upon deep lithiation. Some peaks on figure 11 have not been identified, but could be assigned to lithiated V_2O_5. However, due to the richness of crystalline V_2O_5 phases, singular identification was not possible. Finally, no peaks from crystalline TiO_2 were observed, but a single peak of $LiTiO_2$ was observed. The $LiTiO_2$ (220) reflection was observed as a shoulder on the TiN (200) reflection for the TiO_2-coated samples, and not for the uncoated samples. Amorphous TiO_2 is known to crystallize upon lithiation and delithiation.[54,55] As no electrochemical signature of TiO_2 is found during cycling, we hypothesize that the TiO_2 is lithiated during the first cycle, and acts as a solid electrolyte for the subsequent cycles. The two overlapping peaks of V_2O_5 around 51° in 2theta were chosen to integrate as to not have any interference from other diffraction peaks from lithiated vanadium pentoxide, and the resulting integrated peak intensity shows that the uncoated V_2O_5/CNTS is clearly much more crystalline after electrochemical cycling when compared to the coated samples. This result suggests that the TiO_2 ALD layer does not only act as vanadium dissolution barrier, but also assists in gradually amorphisizing the underlying V_2O_5. We hypothesize that this may be related to internal stress building within these films. Upon charging,

the vanadium oxide undergoes a volume expansion due to the insertion of lithium. The coated samples could buffer this volume expansion to some extent, which causes the vanadium oxide films to be stressed, possibly contributing to the amorphization upon cycling. As elaborated earlier, this also enhances the kinetics, which yields higher capacities at high C-rates. This result explains the increase in capacity observed for the 25 ALD cycles TiO_2 V_2O_5/CNTs seen in Figure 7.

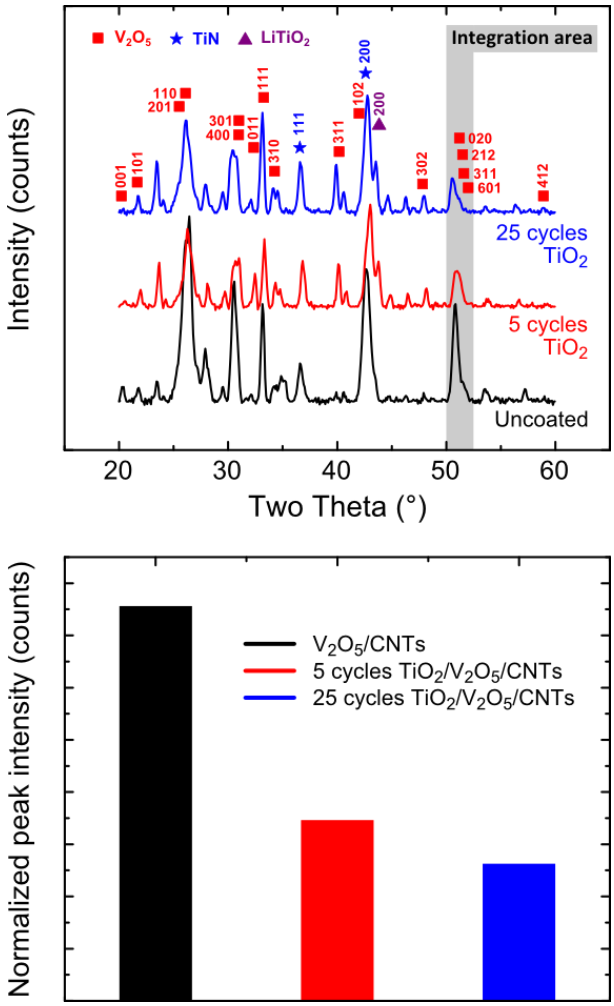

Figure 11. (top) XRD pattern of the post-electrochemical cycling (after 100 charge-discharge cycles, discharged galvanostatically to 4.00V *vs* Li^+/Li) uncoated and coated V_2O_5/CNTs samples. The XRD intensity was normalized to the amount of vanadium remaining after electrochemical

cycling, to allow for direct comparison. The gray area was used to integrate the neighboring (020), (212), (511) and (601) peaks and integrated intensities are plotted (bottom).

4. Conclusion

Heterogeneous TiO_2/V_2O_5/CNTs electrodes were prepared with 5-25 cycles ALD of TiO_2 onto V_2O_5/CNTs, and their electrochemical performance as the cathode electrode of LIBs was evaluated. Different TEM techniques were performed to explain the structural and morphological changes that occurred during the electrochemical tests. A MWCNT-forest template was used as a conductive layer between the substrate and active material (V_2O_5), providing both mechanical support and an increased surface area. Cyclic voltammetry showed faster kinetics for uncoated and 5 ALD cycles TiO_2 coated V_2O_5/CNT samples and slower kinetics for 25 ALD cycles TiO_2 on V_2O_5/CNTs sample. 25 ALD cycles TiO_2 on V_2O_5/CNTs sample also exhibited broad peaks in the CV, which might be an indication of homogeneous filling of V_2O_5. This was also observed with discharge capacity experiments between 1-100C, which showed highest capacity for 25 ALD cycles TiO_2 on V_2O_5/CNTs sample. The delithiation capacity of the electrodes were tested by electrochemical cycling at 2C and showed higher capacity retention for 25 ALD cycles TiO_2 on V_2O_5/CNTs after 100 electrochemical cycles than for uncoated and 5 ALD cycles TiO_2 coated V_2O_5/CNTs. Furthermore, EDX-STEM analysis showed that introducing an additional TiO_2 layer onto V_2O_5/CNTs led to a barrier to the vanadium dissolution. Amorphisation of the V_2O_5 over electrochemical cycling, induced by this lack of vanadium dissolution, enables better kinetics and thus higher available capacity after electrochemical cycling.

ASSOCIATED CONTENT

Supporting Information.

The following files are available free of charge.

Movie M1 shows the electron tomography movie from the TiO_2 coated V_2O_5/CNTs prior to LIB tests (MPEG)

Figure S1 shows the overview of the synthesis route for obtaining heterogeneous TiO_2/V_2O_5/MWCNTs as discussed in this paper.

Figures S2 and S3 show the measured capacities for the kinetics and cyclability, respectively, not scaled to the amount of vanadium XRF counts

Figures S4-S6 show the derivative potential profiles during the first and last (de)lithiation of the samples (PDF)

AUTHOR INFORMATION

Corresponding Author

The corresponding author: Sara Bals, Address: EMAT, University of Antwerp, Groenenborgerlaan 171, B-2020 Antwerp, Belgium, Telephone Number: +32 (0)32653284, E-mail Address: sara.bals@uantwerpen.be.

Author Contributions

The manuscript was written through contributions of all authors. All authors have given approval to the final version of the manuscript. ‡These authors contributed equally.

Funding Sources

This research was funded by the Flemish research foundation FWO-Vlaanderen, by the European Research Council (Starting Grant No. 239865 and No. 335078), by IWT-Flanders (SBO project IWT 18142 “SoS-Lion”) and by the Special Research Fund BOF of Ghent University (GOA - 01G01513).

REFERENCES

1. Bates, J. B.; Dudney, N. J.; Neudecker, B.; Ueda, A.; Evans, C. D. Thin-Film Lithium and Lithium-Ion Batteries, *Solid State Ionics*, **2000**, *135*, 33-45.

2. Roberts, M.; Johns, P.; Owen, J.; Brandell, D.; Edstrom, K.; Enany, G. E.; Guery, C.; Golodnitsky, D.; Lacey, M.; Lecoeur, C.; Mazor, H.; Peled, E.; Perre, E.; Shaijumon, M. M.; Simon, P.; Taberna, P. –L. 3D Lithium Ion Batteries—From Fundamentals to Fabrication, *J. Mater. Chem.,* **2011**, 21, 9876.

3. Oudenhoven, J. F. M.; Baggetto, L.; Notten, P. H. L. All-Solid-State Lithium-Ion Microbatteries: A Review of Various Three-Dimensional Concepts, *Adv. Energy Mater.*, **2010**, 1, 10-33.

4. Baggetto, L.; Niessen, R. A. H.; Roozeboom, F.; Notten, P. H. L. High Energy Density All-Solid-State Batteries: A Challenging Concept Towards 3D Integration, *Adv. Funct. Mater.*, **2008**, 18, 1057-1066.

5. Jiang, J.; Li, Y.; Liu, J.; Huang, X.; Yuan, C.; Lou, X. W. Recent Advances in Metal Oxide-Based Electrode Architecture Design for Electrochemical Energy Storage, *Adv. Mater.*, **2012**, 24, 5166-5180.

6. Leskela, M.; Ritala, M. Atomic Layer Deposition (ALD): From Precursors to Thin Film Structures, *Thin Solid Films*, **2002**, 409, 138-146.

7. Leskela, M.; Ritala, M. Atomic Layer Deposition Chemistry: Recent Developments and Future Challenges, Angew. Chem. Int. Ed., **2003**, 42, 5548 –5554.

8. George, S. M. Atomic Layer Deposition: An Overview, *Chem. Rev.*, **2010**, 110, 111-131.

9. Miikkulainen, V.; Leskela, M.; Ritala, M.; Puurunen, R. L. Crystallinity of Inorganic Films Grown by Atomic Layer Deposition: Overview and General Trends, *J. Appl. Phys.*, **2013**, 113, 021301.

10. Puurunen, R. L. Surface Chemistry of Atomic Layer Deposition: A Case Study for the Trimethylaluminum/Water Process, *Appl. Phys. Rev.*, **2005**, 97, 121301.

11. Chen, X.; Zhu, H.; Chen, Y.; Shang, Y.; Cao, A.; Hu, L.; Rubloff, G. W. MWCNT/V_2O_5 Core/Shell Sponge for High Areal Capacity and Power Density Li-Ion Cathodes, *ACS Nano*, **2012**, 6, 7948–7955.

12. Chen, X.; Pomerantseva, E.; Gregorczyk, K.; Ghodssi, R.; Rubloff, G. Cathodic ALD V_2O_5 Thin Films for High-Rate Electrochemical Energy Storage, **RSC Adv.**, **2013**, 3, 4294-4302.

13. Moriguchl, I.; Hidaka, R.; Yamada, H.; Kudo, T.; Murakami, H.; Nakashima, N. A Mesoporous Nanocomposite of TiO_2 and Carbon Nanotubes as a High-Rate Li-Intercalation Electrode Material, *Adv. Mater.*, **2006**, 18, 69–73.

14. Liu, J.; Sun, X. Elegant Design of Electrode and Electrode/Electrolyte Interface in Lithium-Ion Batteries by Atomic Layer Deposition, *Nanotechnology*, **2015**, 26, 024001.

15. Meng, X.; Yang, X.-Q.; Sun, X. Emerging Applications of Atomic Layer Deposition for Lithium-Ion Battery Studies, *Adv. Mater.*, **2012**, 24, 3589-3615.

16. Ahmed, B.; Xia, C.; Alshareef, H. N. Electrode Surface Engineering by Atomic Layer Deposition: A Promising Pathway Toward Better Energy Storage, *Nano Today*, **2016**, 11, 250-271.

17. Xie, M.; Sun, X.; Sun, H.; Porcelli, T.; George, S. M.; Zhou, Y.; Lian, J. Stabilizing an Amorphous V_2O_5/Carbon Nanotube Paper Electrode with Conformal TiO_2 Coating by Atomic Layer Deposition for Lithium Ion Batteries, *J. Mater. Chem. A.*, **2016**, 4, 537.

18. Whittingham, M. S.; Song, Y.; Lutta, S.; Zavalij, P. Y.; Chernova, N. A. Some Transition Metal(oxy)phosphates and Vanadium Oxides for Lithium Batteries, *J. Mater. Chem.*, **2005**, 15, 3362.

19. Wang, Y.; Cao, G. Developments in Nanostructured Cathode Materials for High-Performance Lithium-Ion Batteries, *Adv. Mater.*, **2008**, 20, 2251–2269.

20. Fang, W.-C.; Fang, W.-L. Fast and Reversible Surface Redox Reduction in V_2O_5 Dispersed on CN_x Nanotubes, *Chem. Commun.*, **2008**, 5236–5238.

21. Chan, C. K.; Peng, H.; Twesten, R. D.; Jarausch, K.; Zhang, X. F.; Cui, Y. Fast, Completely Reversible Li Insertion in Vanadium Pentoxide Nanoribbons, *Nano Lett.*, **2007**, 7, 490–495.

22. Yu, D.; Chen, C.; Xie, S.; Liu, Y.; Park, K.; Zhou, X.; Zhang, Q.; Li, J.; Cao, G. Mesoporous Vanadium Pentoxide Nanofibers with Significantly Enhanced Li-Ion Storage Properties by Electrospinning, *Energy Environ. Sci.*, **2011**, 4, 858.

23. Murhpy, D. W.; Christian, P. A.; Disalvo, F. J.; Waszczak, J. V. Lithium Incorporation by Vanadium Pentoxide, *Inorg. Chem.*, **1979**, 18, 2800-2803.

24. Coustier, F.; Hill, J.; Owens, B. B.; Passerini, S.; Smyrl, W. H. Doped Vanadium Oxides as Host Materials for Lithium Intercalation, *J. Electrochem. Soc.*, **1999**, 146(4), 1355-60.

25. Livage, J. Vanadium Pentoxide Gels, *Chem. Mater.*, **1991**, 3(4), 578-593.

26. Potiron, E.; La Salle, A. L. G.; Verbaere, A.; Piffard, Y.; Guyomard, D. Electrochemically Synthesized Vanadium Oxides as Lithium Insertion Hosts, *Electrochim. Acta*, **1999**, 45(1), 197-214.

27. Lantelme, F.; Mantoux, A.; Groult, H.; Lincot, D. Electrochemical Study of Phase Transition Processes in Lithium Insertion in V_2O_5 Electrodes, *J. Electrochem. Soc.*, **2003**, 150(9), A1202-A1208.

28. Shin, J.; Jung, H.; Kim, Y.; Kim, J. Carbon-Coated V_2O_5 Nanoparticles with Enhanced Electrochemical Performance as a Cathode Material for Lithium Ion Batteries, *J. Alloys Compd.*, **2014**, 589, 322-329.

29. Pan, A.; Wu, H. B.; Yu, L.; Zhu, T.; Lou, X.W. Synthesis of Hierarchical Three-Dimensional Vanadium Oxide Microstructures as High-Capacity Cathode Materials for Lithium-Ion Batteries, *ACS Appl. Mater. Interfaces*, **2012**, 4(8), 3874-3879.

30. Huang, X.; Rui, X.; Hng, H. H.; Yan, Q. Vanadium Pentoxide-Based Cathode Materials for Lithium-Ion Batteries: Morphology Control, Carbon Hybridization, and Cation Doping, *Part. Part. Syst. Charact.*, **2015**, 32(3), 276-294.

31. Leger, C.; Bach, S.; Soudan, P.; Pereira-Ramos, J.-P. Structural and Electrochemical Properties of ω - $Li_xV_2O_5$ ($0.4 \leqslant x \leqslant 3$) as Rechargeable Cathodic Material for Lithium Batteries, *J. Electrochem. Soc.*, **2005**, 152(1), A236-A241.

32. Delmas, C.; Cognac-Auradou, H.; Cocciantelli, J. M.; Menetrier, M.; Doumerc, J. P. The $Li_xV_2O_5$ System: An Overview of the Structure Modifications Induced by the Lithium Intercalation, *Solid State Ionics*, **1994**, 69, 257-264.

33. Yi, T.-F.; Zhu, Y.-R.; Zhu, X.-D.; Shu, J.; Yue, C.-B.; Zhou, A.-N. A Review of Recent Developments in the Surface Modification of $LiMn_2O_4$ as Cathode Material of Power Lithium-Ion Battery, *Ionics*, **2009**, 15, 779-784.

34. Wang, H.-Y.; Wang, F.-M. Electrochemical Investigation of an Artificial Solid Electrolyte Interface for Improving the Cycle-ability of Lithium Ion Batteries Using an Atomic Layer Deposition on a Graphite Electrode, *J. Power Sources*, **2013**, 233, 1-5.

35. Lipson, A. L.; Puntambekar, K.; Comstock, D. J.; Meng, X.; Geier, M. L.; Elam, J. W.; Hersam, M. C. Nanoscale Investigation of Solid Electrolyte Interphase Inhibition on Li-Ion Battery MnO Electrodes via Atomic Layer Deposition of Al_2O_3, *Chem. Mater.*, **2014**, 26, 935-940.

36. Xiao, X.; Ahn, D.; Liu, Z.; Kim, J.-H.; Lu, P. Atomic Layer Coating to Mitigate Capacity Fading Associated with Manganese Dissolution in Lithium Ion Batteries, *Electrochem. Comm.*, **2013**, 32, 31-34.

37. Cheng, H.-M.; Wang, F.-M.; Chu, J. P.; Santhanam, R.; Rick, J.; Lo, S.-C. Enhanced Cycleability in Lithium Ion Batteries Resulting from Atomic Layer Deposition of Al_2O_3 or TiO_2 on $LiCoO_2$ Electrodes, *J. Phys. Chem. C.*, **2012**, 116, 7629-7637.

38. Li, X.; Liu, J.; Meng, X.; Tang, Y.; Banis, M. N.; Yang, J.; Hu, Y.; Li, R.; Cai, M.; Sun, X. Significant Impact on Cathode Performance of Lithium-Ion Batteries by Precisely Controlled Metal Oxide Nanocoatings via Atomic Layer Deposition, *J. Power Sources*, **2014**, 247, 57-69.

39. Jung, Y. S.; Cavanagh, A. S.; Dillon, A. C.; Groner, M. D.; George, S. M.; Lee, S.-L. Enhanced Stability of $LiCoO_2$ Cathodes in Lithium-Ion Batteries Using Surface Modification by Atomic Layer Deposition, *J. Electrochem. Soc.*, **2010**, 157(1), A75-A81.

40. Laskar, M. R.; Jackson, D. H. K.; Guan, Y.; Xu, S.; Fang, S.; Dreibelbis, M.; Mahanthappa, M. K.; Morgan, D.; Hamers, R. J.; Kuech, T. F. Atomic Layer Deposition of Al_2O_3–Ga_2O_3 Alloy Coatings for $Li[Ni_{0.5}Mn_{0.3}Co_{0.2}]O_2$ Cathode to Improve Rate Performance in Li-Ion Battery, *ACS Appl. Mater. Interfaces*, **2016**, 8, 10572-10580.

41. Lee M.-L.; Su, C.-Y.; Lin, Y.-H.; Liao, S.-C.; Chen, J.-M.; Perng, T.-P.; Yeh, J.-W.; Shih, H. C. Atomic Layer Deposition of TiO_2 on Negative Electrode for Lithium Ion Batteries, *J. Power Sources*, **2013**, 244, 410-416.

42. Chiodarelli, N.; Masahito, S.; Kashiwagi, Y.; Li, Y.; Arstila, K.; Richard, O.; Cott, D. J.; Heyns, M.; De Gendt, S.; Groeseneken, G.; Vereecken, P. M. Measuring the Electrical Resistivity and Contact Resistance of Vertical Carbon Nanotube Bundles for Application as Interconnects, **Nanotechnology**, **2011**, 22, 085302.

43. Deng, S.; Verbruggen, S. W.; He, Z.; Cott, D. J.; Vereecken, P. M.; Martens, J. A.; Bals, S.; Lenaerts, S.; Detavernier, C. Atomic Layer Deposition-Based Synthesis of Photoactive TiO_2 Nanoparticle Chains by Using Carbon Nanotubes as Sacrificial Templates, *RSC Adv.*, **2014**, 4, 11648.

44. Deng, S.; Kurttepeli, M.; Cott, D. J.; Bals, S.; Detavernier, C. Porous Nanostructured Metal Oxides Synthesized Through Atomic Layer Deposition on a Carbonaceous Template Followed by Calcination, *J. Mater. Chem. A*, **2015**, 3, 2642–2649.

45. Kurttepeli, M.; Deng, S.; Verbruggen, S.W.; Guzzinati, G.; Cott, D.J.; Lenaerts, S.; Verbeeck, J.; Van Tendeloo, G.; Detavernier, C.; Bals, S. Synthesis and Characterization of Photoreactive TiO_2–Carbon Nanosheet Composites, *J. Phys. Chem. C*, **2014**, 118(36), 21031-21037.

46. Borghols, W. J. H.; Lutzenkirchen-Hecht, D.; Haake, U.; Chan, W.; Lafont, U.; Kelder, E. M.; Van Eck, E. R. H.; Kentgens, A. P. M.; Mulder, F. M.; Wagemaker, M. Lithium Storage in Amorphous TiO_2 Nanoparticles, *J. Electrochem. Soc.*, **2010**, 157 (5), A582-A588.

47. Koltypin, M.; Pol, V.; Gedanken, A.; Aurbach, D. The Study of Carbon-Coated V_2O_5 Nanoparticles as a Potential Cathodic Material for Li Rechargeable Batteries, *J. Electrochem. Soc.*, **2007**, 154, A605.

48. Odani, A.; Pol, V. G.; Pol, S. V.; Koltypin, M.; Gedanken, A.; Aurbach, D. Testing Carbon-Coated VO_x Prepared via Reaction under Autogenic Pressure at Elevated Temperature as Li-Insertion Materials, *Adv. Mater.*, **2006**, 18, 1431–1436.

49. Liu D.; Liu, Y.; Candelaria, S. L.; Cao, G.; Liu, J.; Jeong, Y.-H. Atomic Layer Deposition of Al_2O_3 on V_2O_5 Xerogel Film for Enhanced Lithium-Ion Intercalation Stability, *J. Vac. Sci. Technol.*, **2012**, 30, 01A123.

50. West, K.; Zachau-Christiansen, B.; Jacobsen, T.; Skaarup, S. Vanadium Oxide Xerogels as Electrodes for Lithium Batteries, *Electrochim. Acta*, **1993**, 38, 1215–1220.

51. Julien, C.; Nazri, G.-A.; *Solid State Batteries: Materials Design and Optimization*, Springer US, LLC, 1994.

52. Fang, H.-T.; Liu, M.; Wang, D.-W.; Sun, T.; Guan, D.-S.; Li, F.; Zhou, J.; Sham, T.-K.; Cheng, H.-M. Comparison of the Rate Capability of Nanostructured Amorphous and Anatase TiO_2 for Lithium Insertion Using Anodic TiO_2 Nanotube Arrays, *Nanotechnology*, **2009**, 20, 225701.

53. McGraw, J. M.; Perkins, J. D.; Zhang, J.-G.; Liu, P.; Parilla, P. A.; Turner, J.; Schulz, D. L.; Curtis, C. J.; Ginley, D. S. Next Generation V_2O_5 Cathode Materials for Li Rechargeable Batteries, *Solid State Ionics*, **1998**, 113-115, 407-413.

54. Xiong, H., Yildirim, H., Shevchenko, E.V., Prakapenka, V.B., Koo, B., Slater, M.D., Balasubramanian, M., Sankaranarayanan, S.K.R.S., Greeley, J.P., Tepavcevic, S., Dimitrijevic, N.M., Podsiadlo, P., Johnson, C.S., Rajh, T., 2012. Self-Improving Anode for Lithium-Ion Batteries Based on Amorphous to Cubic Phase Transition in TiO_2 Nanotubes, *J. Phys. Chem. C*, 116, 3181–3187.

55. González, J.R., Alcántara, R., Nacimiento, F., Ortiz, G.F., Tirado, J.L., 2015. Relationships Between the Length of Self-Organized Titania Nanotube Adsorbed Solvents and its Electrochemical Reaction with Lithium, *J. Solid State Electrochem.*, **2015**, 19, 3013–3018.

Supporting Information

Heterogeneous TiO_2/V_2O_5/Carbon Nanotube Electrodes for Lithium-Ion Batteries

*Mert Kurttepeli[1, ‡], Shaoren Deng[2, ‡], Felix Mattelaer[2, ‡], Daire J. Cott[3], Philippe Vereecken[3], Jolien Dendooven[2], Christophe Detavernier[2] and Sara Bals[1, *]*

[1] Department of Physics, Electron Microscopy for Materials Science (EMAT), University of Antwerp, Groenenborgerlaan 171, B-2020 Antwerp, Belgium

[2] Department of Solid State Sciences, Ghent University, Krijgslaan 281 S1, B-9000 Gent, Belgium

[3] IMEC, Kapeldreef 75, B-3001 Leuven, Belgium

[*]The corresponding author: Sara Bals, Address: EMAT, University of Antwerp, Groenenborgerlaan 171, B-2020 Antwerp, Belgium, Telephone Number: +32 (0)32653284, E-mail Address: sara.bals@uantwerpen.be.

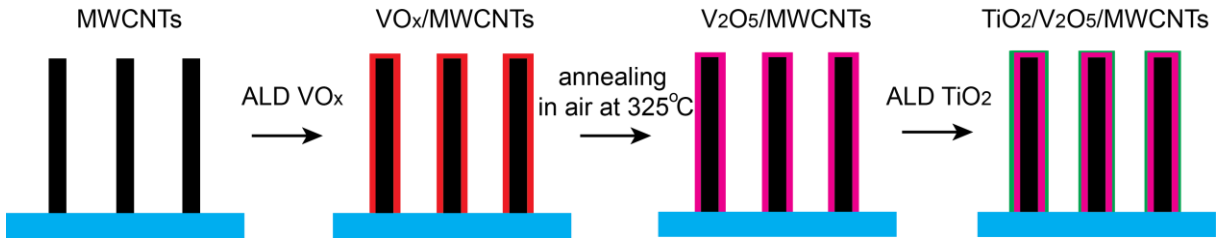

Figure S1. Overview of the synthesis route for obtaining heterogeneous TiO_2/V_2O_5/MWCNTs as discussed in this paper. VO_x metal oxide were coated on MWCNTs by ALD. Subsequent annealing in air at 325°C causes the transformation of the VO_x coating into V_2O_5 without the removal of MWCNTs. An extra layer of TiO_2 were coated onto VO_x/MWCNTs, which resulted in obtaining the heterogeneous TiO_2/V_2O_5/MWCNTs material.

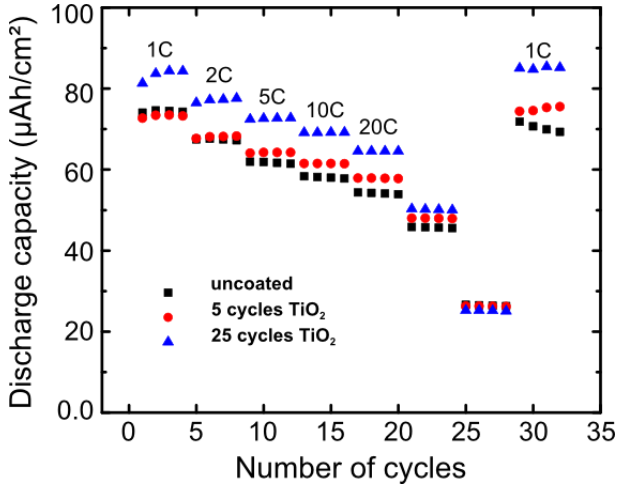

Figure S2. Discharge capacity of the kinetics at 1-100C for 30 electrochemical cycles of uncoated and 5 and 25 ALD cycles TiO_2 coated V_2O_5/CNTs. C-rates were calculated based on the measured vanadium content of the samples.

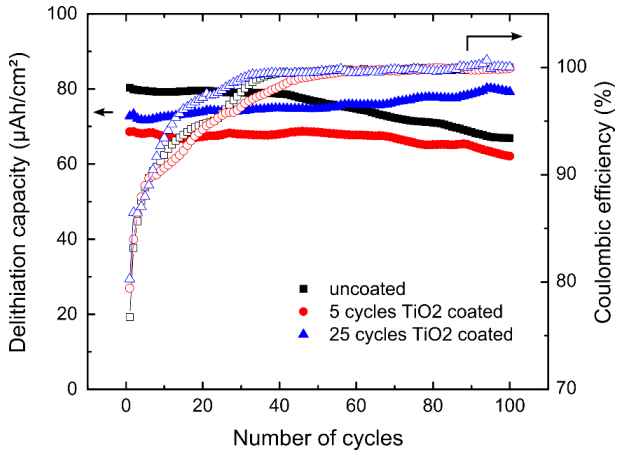

Figure S3. Cyclability testing of uncoated V_2O_5/CNTs and of 5 and 25 ALD cycles TiO_2 on V_2O_5/CNTs samples at a current corresponding to 2C between 2.0 and 4.0 V vs Li^+/Li.

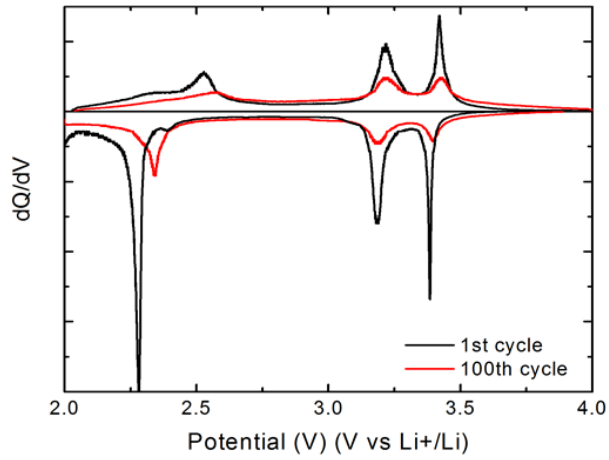

Figure S4. Derivative potential profile of the uncoated V_2O_5/CNTS during the first and 100th lithiation (negative dQdV) and delithiation (positive dQdV).

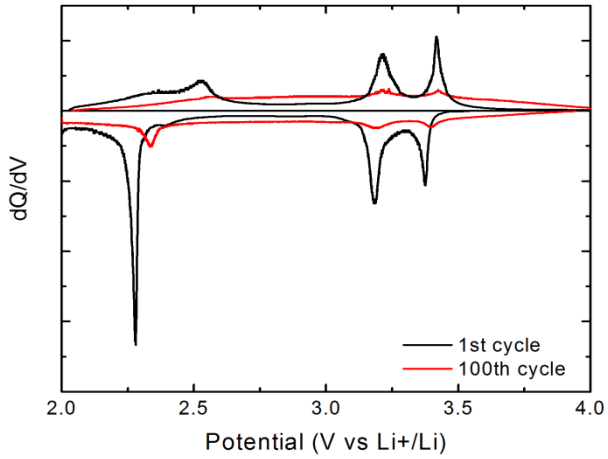

Figure S5. Derivative potential profile of the 5 ALD cycles TiO_2 coated V_2O_5/CNTS during the first and 100th lithiation (negative dQdV) and delithiation (positive dQdV).

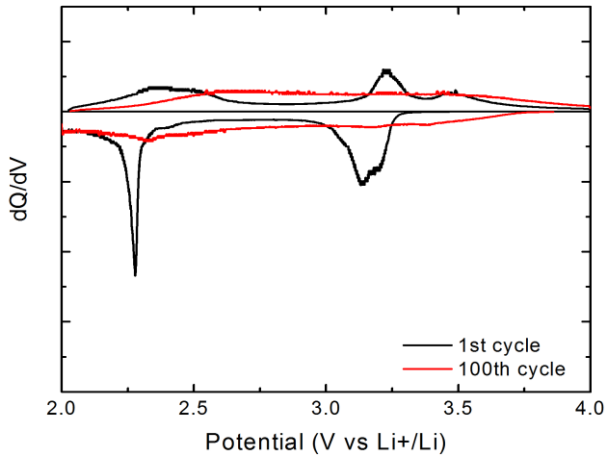

Figure S6. Derivative potential profile of the 25 ALD cycles TiO_2 coated V_2O_5/CNTS during the first and 100th lithiation (negative dQdV) and delithiation (positive dQdV).